Polarization effects in coherent scattering from magnetic specimen: Implications for x-ray holography, lensless imaging, and correlation spectroscopy

S. Eisebitt,* M. Lörgen, and W. Eberhardt
BESSY mbH, Albert-Einstein-Str. 15, D-12489 Berlin, Germany

J. Lüning and J. Stöhr
SSRL, Stanford Linear Accelerator Center, 2575 Sand Hill Road, Menlo Park, California 94025, USA

C. T. Rettner and O. Hellwig
IBM Corp., Almaden Research Center, 650 Harry Road, San Jose, California 95120, USA

E. E. Fullerton
San Jose Research Center, Hitachi Global Storage Technologies, 650 Harry Road, San Jose, California 95037, USA

G. Denbeaux
Center for X-ray Optics, E. O. Lawrence Berkeley National Laboratory, 1 Cyclotron Road, Berkeley, California 94720, USA
(Received 10 March 2003; published 18 September 2003)

We present resonant coherent small-angle scattering from sub-μm magnetic domains in an in-line holography geometry. By varying the polarization of the incident soft x rays the interference between the reference wave propagating from a pinhole and scattered object wave can be switched ''on'' or ''off.'' The reference-object interference contribution in the scattering can be isolated by combining measurements with right and left circular polarizations. The implications for spatial and temporal interference experiments of magnetic specimen such as holography, lensless imaging, or photon correlation spectroscopy are discussed.

DOI: 10.1103/PhysRevB.68.104419 PACS number(s): 78.70.Ck, 75.70.Kw, 61.10.Eq

In a holographic experiment the phase information is recorded via the interference of the wave scattered by the specimen (object wave) with a known reference wave.[1] Under the proper conditions, three-dimensional sample information is encoded in the hologram. Holography is a special application of coherent scattering. Recently there has been great interest in exploring various methods of ''lensless'' imaging with coherent x rays. A method that has received particular attention is nonholographic in nature, combining coherent x-ray scattering with oversampling techniques to retrieve the phase information and reconstruct the image.[2–5] All coherent x-ray interference techniques can, in principle, achieve a spatial resolution on the order of the wavelength of the electromagnetic radiation. The use of extreme ultraviolet (EUV) or soft x-ray (SX) radiation with wavelengths in the nanometer range therefore provides access to the world of nanostructures. Holograms of nonmagnetic specimens have been recorded in the EUV (Ref. 6) and SX (Refs. 7–9) wavelength range in the past.

To our knowledge, magnetic materials have so far not been imaged by x-ray holography or oversampling phasing techniques. The study of magnetic effects on a nanometer scale has become an area of great scientific and technological importance. The fundamentals of nanomagnetism are currently being studied with respect to static effects such as magnetic coupling or domain-wall geometries and with respect to dynamic processes such as switching or demagnetization.[10] Current hard drive data storage technology relies on thin magnetic films of a few nm thickness and magnetic coupling effects between different magnetic layers such as exchange bias. Additional lateral structuring of magnetic storage media on the nm scale is one possible future route for higher storage densities.[11]

For the study of magnetic materials, the SX wavelength range is especially appealing, as core-level resonances can be exploited to probe magnetic properties with element specifity, i.e., the individual magnetic properties of the constituents in complex magnetic systems can be probed separately.[12] Furthermore, the cross sections for resonant magnetic scattering of x rays are high and can be exploited to generate magnetic contrast for both ferromagnetic and antiferromagnetic materials.[13,14] At the $L_{2,3}$ absorption edges of Fe and Co, the magnetic contrast is as high as 50%.[15–17] Coherent magnetic soft x-ray scattering has recently been utilized to investigate domain structures[18–21] and the microscopic origins of magnetic hysteresis.[22,23]

In this paper we focus on the basic question of how the polarization dependencies in the x-ray resonant magnetic scattering cross section influence interference experiments such as x-ray holography or imaging by oversampling phasing. Coherent magnetic scattering from sub-μm domains in in-line geometry is presented. We will demonstrate that it is important for a magnetic specimen to take into account polarization effects in the interference between reference wave and magnetically scattered wave in order to acquire suitable experimental data for both types of experiments.

The polarization dependence in charge and resonant magnetic x-ray scattering is expressed in the following representation of the complex scattering factors f^n for a scattering center n,[24,25]

$$f^n=(\mathbf{e}'\cdot\mathbf{e})f_c^n+i(\mathbf{e}'\times\mathbf{e})\cdot\mathbf{M}^n f_{m1}^n+(\mathbf{e}'\cdot\mathbf{M}^n)(\mathbf{e}\cdot\mathbf{M}^n)f_{m2}^n, \quad (1)$$

where **e** and **e**′ are the polarization vectors of the incident and scattered x rays, respectively, and **M**(**r**) is the magnetization vector at a given sample point. f_c and f_m are scattering factors for charge and magnetic scattering, evaluated by dipole matrix elements from the initial to the final state.[24–26]

The measured intensity is $I(\mathbf{q})=|\Sigma_n f^n e^{i\mathbf{q}\mathbf{r}_n}|^2$ where **q** is the photon wave-vector transfer in the scattering process and the summation over the scatterers located at $\mathbf{r}_n$ runs over a coherence volume in the sample. The magnetic terms containing f_{m1} and f_{m2} in Eq. (1) give rise to circular and linear x-ray magnetic dichroism in the scattered or absorbed x-ray intensity.

Electromagnetic waves with orthogonal polarization states cannot interfere, i.e., the time average of the interference term does not contribute to the intensity. In order to optimize interference for holography or homo/heterodyning in dynamic experiments it is thus important to take the polarization dependencies in the scattering cross sections into account. This is particularly important in resonant magnetic scattering due to the complex polarization dependence of the scattering cross section described by Eq. (1).

Let us first discuss the situation for spatial interference in a holographic experiment. In Gabor or in-line holography, a spherical wave is created by illumination of a sufficiently small pinhole. The sample is illuminated by the spherical wave and the interference between the undisturbed spherical wave and the wave scattered from the sample is observed. We have performed an experiment in this geometry [Fig. 1(a)], exploiting the resonant magnetic small-angle scattering from magnetic worm domains in a thin-film medium with perpendicular magnetic anisotropy. The measurements were done at the BESSY storage ring on beam line UE-56/1, which is equipped with an elliptical polarization undulator and a SGM monochromator. The sample consists of a magnetic multilayer on a SiN_x membrane of 160 nm thickness with the composition Pt(20 nm)/[Co(3 nm)/Pt(0.7 nm)]$_{50}$/Pt(2 nm), grown by magnetron sputtering.[35] This structure leads to a remanent state of lateral worm domains, with the magnetization in each domain being either parallel or antiparallel to the sample normal. A transmission x-ray microscopy image of the sample using circular dichroism to generate magnetic contrast is shown in Fig. 1(c).[36] A 2.5-μm-diameter pinhole in a free-standing gold film of 2.0 μm thickness, located 380 μm in front of the sample restricted the sample illumination to a volume smaller than the coherence volume of the x-ray beam at the sample position, which was 6.4 μm (longitudinal)$\times$612 μm (transverse vertical)$\times$5.6 μm (transverse horizontal). Great care was taken to fabricate a high quality pinhole using a focused ion beam of 30-keV Ga^+ ions [Fig. 1(b)]. The cut was made in two steps using custom scripts to control the beam. First a 70-pA beam was used to cut a ''rough'' 2.3-μm hole, then the opening was enlarged and fine polished with a 4-pA beam that slowly spiralled outwards to the 2.5-μm diameter.[37]

In Figs. 2(a)–(c), we present coherent scattering patterns obtained for incident radiation of (a) linear polarization, (b) right circular polarization, and (c) left circular polarization. The experiments were performed with an x-ray wavelength

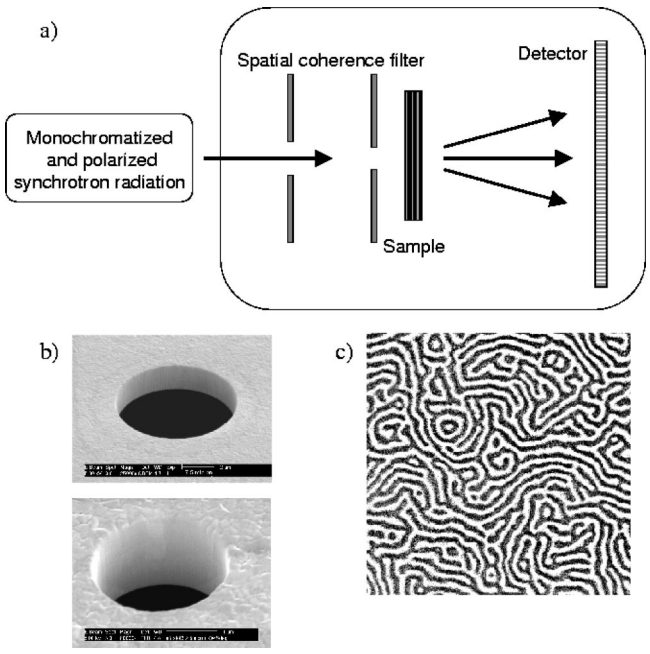

FIG. 1. (a) Scheme of the experimental setup for coherent resonant magnetic small-angle scattering at a synchrotron beamline. Soft x rays are generated with full polarization control in an APPLE-II undulator at BESSYII. The longitudinal coherence is increased by energy filtering in the beamline with $\lambda/\Delta\lambda=4000$. The transverse coherence length at the sample are defined by the beamline optics and geometry of the setup. The vertical source size is 10 μm 7700 mm upstream of the sample, the horizontal source size is 1000 μm 7000 mm upstream of the sample. The scattered radiation is detected on a microchannelplate detector with resistive anode readout for 2D spatial resolution. The total active area is 40 mm$\times$40 mm with 100 μm$\times$100 μm resolution elements. The sample – detector distance is 894 mm. (b) Pinholes for spacial coherence filtering fabricated by a focused ion beam of 30-keV Ga^+ ions in a free-standing Au film of 2 μm thickness. The scanning electron microscopy images show a pinhole of 7.5 μm (top) and 2.5 μm diameter (bottom). (c) Soft x-ray microscopy image of a 5 μm$\times$5 μm region of our sample, recorded at the ALS XM-1 microscope. Magnetic contrast is obtained by circular dichroism described by the f_{m1} term in Eq. (1) (Ref. 34). Magnetic worm domains are clearly visible. The magnetization is directed out of (white) or into (black) the image plane.

of 1.59 nm (778 eV), corresponding to resonant scattering at the Co L_3 edge. The sample normal was oriented parallel to the wave vector of the incident radiation. As seen in Fig. 2(a), the scattering pattern consists of a Fraunhofer pattern due to the scattering from the pinhole and a ''ring'' of intensity centered at $q=0$ with a broad peak in the radial distribution at $q=32$ μm^{-1}, in agreement with the radial distribution obtained from the x-ray microscope image. The peak corresponds to an in-plane correlation length of 196 nm. The observed scattered intensity is due to magnetic small-angle scattering, produced by the difference in scattering factors from oppositely magnetized domains according to the second term in Eq. (1).[26] Due to our experimental geometry, the third term in Eq. (1) vanishes as $(e\cdot M^n)$ is always zero for domains magnetized (anti)parallel to the sample normal. The

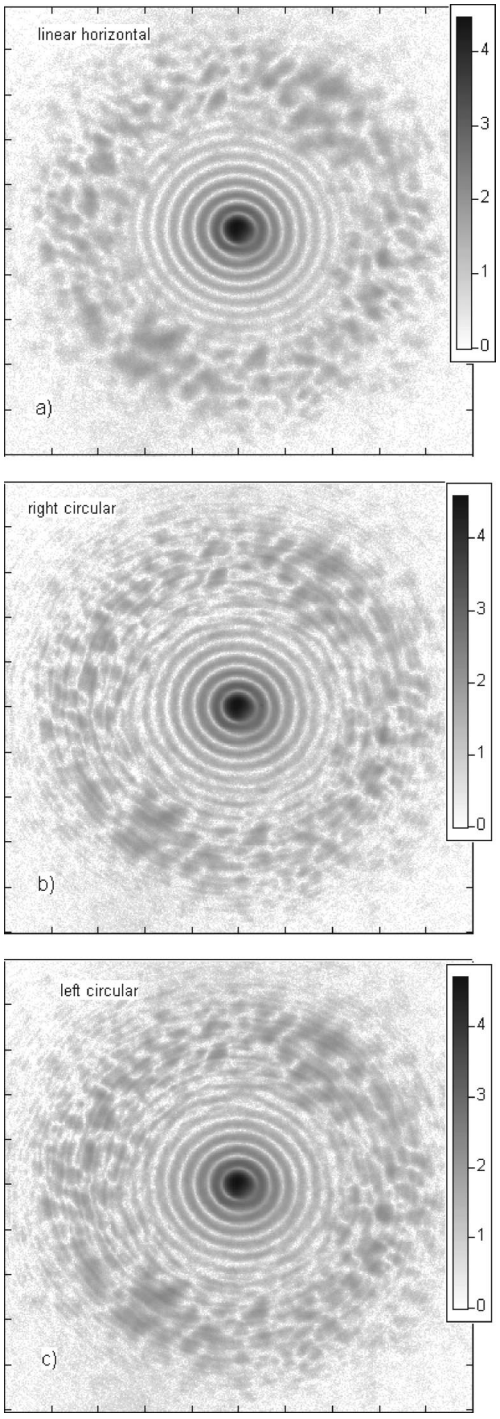

FIG. 2. Coherent resonant small-angle scattering patterns recorded with soft x rays of 1.59-nm wavelength, corresponding to the Co $2p_{3/2} \rightarrow$ valence-band scattering resonance. The scale range of both horizontal and vertical axes is $-50\ \mu\mathrm{m}^{-1}$ to $50\ \mu\mathrm{m}^{-1}$ of in-plane momentum transfer. The unscattered reference wave from the 2.5-μm-diameter pinhole gives rise to a Fraunhofer pattern, while resonant magnetic scattering from the domain distribution gives rise to a ring of intensity broken up in individual speckle. Intensity is represented in a logarithmic greyscale. With incident radiation of linear polarization (a), no interference between reference and object wave can be observed. Interference can occur for an incident x-ray beam of right (b) and left (c) circular polarization.

second term is nonzero and changes its sign between oppositely magnetized domains. The scattering factor for small-angle scattering thus has a magnitude of $2M_n f_{m1}$.[26] As the scattering is coherent, the intensity is broken up into individual speckles. The speckle visibility defined as $(I_{max} - I_{min})/(I_{max} + I_{min})$ for adjacent maxima and minima is about 0.9. This implies a very high degree of coherence, in agreement with a contrast value of $\beta = 0.9$ as independently determined by the intensity standard deviation divided by the mean intensity in a **q**-space region containing several speckles.[27,28] The magnetic small-angle scattering vanishes when the photon energy is tuned 20 eV below the Co L_3 absorption resonance, corroborating the magnetic nature of this feature. Within the ± 80-$\mu\mathrm{m}^{-1}$ in-plane momentum transfer covered by our detector, we do not detect any charge scattering due to sample roughness. This is in accord with scanning tunneling microscopy studies of the sample which indicate a surface rms roughness less than 5 nm with in-plane correlation lengths smaller than 50 nm. Since many Fraunhofer rings generated by the pinhole are visible in the q range containing magnetic scattering it is difficult to perform a holographic image reconstruction due to the many phase changes of the reference wave. A smaller diameter pinhole will resolve this problem. Nevertheless, polarization effects in the interference pattern and their consequences for spatial or temporal interference experiments can be illustrated.

For incident radiation with *linear* polarization, there is *no* interference between the unscattered reference wave propagating from the pinhole and the magnetic scattering from the domain distribution. This is due to the fact that diffraction by the pinhole does not change the polarization of the radiation while the f_{m1} term in the resonant magnetic scattering cross section is maximized when the plane of polarization for linearly polarized radiation is rotated by $\pi/2$. As a result, unscattered and magnetically scattered radiation go into orthogonal polarization channels and cannot interfere.

The fact that the pinhole wave and magnetically scattered sample wave are merely superimposed in intensities in the detector image shown in Fig. 2(a) can be seen more clearly when considering a situation where interference between pinhole wave and magnetically scattered wave is possible. Circular polarization is an eigenstate of the f_{m1} term in Eq. (1). Right (left) circular polarized x rays are scattered into the same polarization state and can consequently interfere with the pinhole wave at the detector. A coherent scattering image recorded with incident right circular polarized radiation (the degree of polarization is 85%) is presented in Fig. 2(b). All other experimental parameters were kept constant. Reference wave – object wave interference structures can clearly be observed in the detector image. The existence of this interference is crucial for all magnetic x-ray holography experiments. In a dynamic experiment, this interference would be exploited as a homodyning between the scattering signal and the source oscillator.

When the polarization is changed to left circular, we observe the intensity distribution presented in Fig. 2(c). For each type of magnetic domain, the contribution associated with the $[i(\mathbf{e}' \times \mathbf{e}) \cdot \mathbf{M}^n f_{m1}^n]$ term in Eq. (1) to the scattering factor changes its sign when the polarization is changed from

right to left circular. As a result, the magnetic sample contrast inverts. The overall small-angle scattering contrast, however, remains the same as adjacent oppositely magnetized domains still differ in their scattering factor by $2M_n f_{m1}$.

While the magnetic contrast from the sample inverts, the diffraction from the pinhole does not change upon helicity reversal. Due to the interference between the reference wave from the pinhole and the resonant magnetically scattered wave we observe a different intensity distribution from the right circular case. If we make the pinhole size significantly larger than the magnetic in-plane correlation length (about 196 nm), e.g., by working with a pinhole of 20-μm diameter, pinhole diffraction and magnetic scattering are to a first approximation separated in **q** space and the beating between reference wave and object wave becomes negligible. In this case, the speckle structure of the magnetic scattering from the sample is unchanged upon helicity reversal (not shown), in agreement with Babinet's theorem.

If the coherent scattering intensities measured with right and left circular polarization are added, all reference-object interference structures cancel and we obtain exactly the intensity distribution as measured with linear polarization. The greyscale images of Figs. 2(b) and (c) can be superimposed manually after copying to a transparency. The summation is shown in Fig. 3(a). This is an illustration of the fact that linear polarization can be thought of as the coherent superposition of right and left circular polarization and that orthogonal polarization channels cannot interfere in the sense that cross terms do not contribute to the time averaged intensity.

In Fig. 3(b), we present the intensity difference between the measurements with right and left circular polarization. This difference pattern is a special kind of hologram. Here, the pure charge scattering and the pure magnetic term cancel out and the difference image is proportional to the reference-magnetic interference terms alone. (Charge scattering from the sample and the resulting interference term can be neglected in our experiment.) The square of the reference wave amplitude and the square of the object wave amplitude are thus removed from the hologram and only the terms giving rise to the virtual and the real image in the holographic image reconstruction are retained. By removing the pure object wave term for magnetic samples in this fashion one can thus diminish the problem associated with samples of insufficient transparency, which, according to Ref. 1,''seriously hampers the use of Gabor holograms in many possible applications.'' In addition, the transparency of the sample for the reference wave can be adjusted in resonant magnetic scattering by slight tuning of the x-ray wavelength in the vicinity of the absorption edge.

Our conclusions regarding the interference between reference and object wave in resonant magnetic scattering also apply to all other holography geometries such as off-axis (Leith Upatnieks) or Fourier transform holography.[1,8] They are also applicable to dynamical experiments using homo/heterodyning, as they only depend on the modification of the polarization of the incident wave by the magnetic scattering. For all reference waves generated by diffracting elements

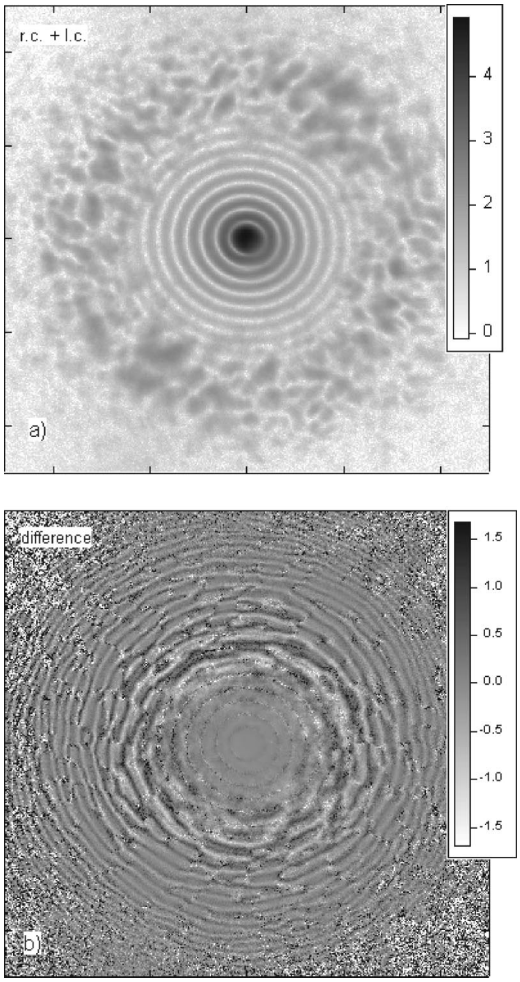

FIG. 3. If the intensities in Figs. 2(b) and (c) are added, one obtains the intensity distribution in Fig. 3(a). Again the axes range from -50 to 50 μm^{-1}. The difference image of both circular polarizations is shown in Fig. 3(b). In the difference image only the reference – magnetic scattering interference structures are visible.

such as pinholes, zone plates or transmission gratings, the incident polarization remains unchanged. In order to observe maximum interference with the reference wave, one has to find an experimental arrangement where the polarization state of the scattered wave has a maximum projection onto the reference wave polarization state.

In phasing oversampling experiments it is often desirable to suppress the diffraction structure from the radiation source such as a pinhole. L-shaped guard slits between the pinhole and the sample are often being used for this reason.[4,29] Guard slits, however, can only shield part of the detector from the pinhole diffraction pattern—otherwise the guard slits themselves would produce a strong diffraction pattern. As a result, diffraction from the sample without superposition of diffraction structures from the pinhole can only be measured in certain regions of **q** space. In magnetic scattering, this problem can be solved by choosing experimental conditions such as in Fig. 2(a) where no interference can be observed. Due to the absence of reference-object interference the Airy pattern generated by the pinhole can then be subtracted by measuring the pinhole alone in a reference experiment.

If the reference beam can be generated by resonant scattering in matter rather than by diffraction, the polarization of the reference x-ray beam itself can be controlled by the polarization dependencies in Eq. (1). For this purpose, the same atomic resonance has to be used in the reference and the sample beam. One could envision magnetized reflective elements such as multilayer mirrors or zone plates. By suitable magnetic engineering, such elements could be optimized for maximum (or minimum) source-sample interference. If the magnetization of the optical element can be changed by an external field, an oscillating magnetic field could be used to modulate the interference signal allowing lock-in detection.

We would like to emphasize that the polarization effects in resonant magnetic scattering which are important for *spatial* interference are just as important in *temporal* interference. Photon correlation spectroscopy [PCS, also known as dynamic light scattering (DLS)] is a prominent technique for the study of dynamics in a wide variety of systems ranging from surface capillary waves to chemical reactions.[30] PCS is typically performed using lasers but has in recent years also been performed in the hard x-ray region.[31] The feasibility of soft x-ray PCS using a third generation synchrotron radiation source has recently been demonstrated with an experiment on liquid crystals.[32] In PCS, the temporal fluctuation of a speckle in the coherent scattering pattern is detected. Heterodyne detection techniques relying on interference in the time domain are standard in PCS experiments using lasers in order to increase the experimental sensitivity. The time-dependent signal to be measured is mixed with a reference wave of known frequency resulting in a mixture of first- and second-order intensity-intensity autocorrelation functions. In this way, the PCS signal which is proportional to the correlation function of the sample can be enhanced considerably. Heterodyne mixing has recently been observed in the hard x-ray regime[33] but has so far not been realized in the EUV or SX regime. In the x-ray regime, the reference wave and the wave incident on the sample have to be generated by the same primary radiation source. Sample and reference wave have to be separated, typically by employing diffractive elements. The situation is thus analogous to the spatial interference case discussed in this paper. The polarization effects discussed in the context of static holographic imaging will also be crucial in the study of magnetization dynamics with PCS using heterodyne detection.

In conclusion, we have performed a resonant coherent magnetic scattering experiment in an in-line holography geometry using resonant x rays of 1.59-nm wavelength. We observe polarization effects in the magnetic scattering that allow us to switch the interference between a soft x-ray reference wave and the magnetically scattered wave ''on'' or ''off.'' By combining measurements with different incident polarizations, we were able to isolate the interference contributions to the coherent scattering. The observed polarization effects are crucial in the investigation of magnetic materials by techniques based on spatial interference (holography, oversampling phasing imaging) or temporal interference (correlation spectroscopy, homo/heterodyning detection) in the x-ray regime.

We thank H. Dürr, J. B. Kortright, S. D. Kevan, and H.-C. Siegmann for valuable discussions. Part of the present work was supported by the Office of Basic Energy Sciences of the U.S. Department of Energy.

*Electronic address: eisebitt@bessy.de

[1] J. Goodman, *Introduction to Fourier Optics* (McGraw-Hill, Inc., New York, 1996), 2nd ed.
[2] R.W. Gerchberg and W.O. Saxton, Optik (Stuttgart) **35**, 237 (1972).
[3] J.R. Fienup, Appl. Opt. **21**, 2758 (1982).
[4] J.W. Miao, P. Charalambous, J. Kirz, and D. Sayre, Nature (London) **400**, 342 (1999).
[5] I.K. Robinson, I.A. Vartanyants, G.J. Williams, M.A. Pfeifer, and J.A. Pitney, Phys. Rev. Lett. **87**, 195505 (2001).
[6] J.E. Trebes, S.B. Brown, E.M. Campbell, D.L. Matthews, D.G. Nilson, G.F. Stone, and D.A. Whelan, Science **238**, 517 (1987).
[7] M. Howells, C. Jacobsen, J. Kirz, R. Feder, K. Mcquaid, and S. Rothman, Science **238**, 514 (1987).
[8] I. McNulty, J. Kirz, C. Jacobsen, E.H. Anderson, M.R. Howells, and D.P. Kern, Science **256**, 1009 (1992).
[9] M.R. Howells, C.J. Jacobsen, S. Marchesini, S. Miller, J.C.H. Spence, and U. Weirstall, Nucl. Instrum. Methods Phys. Res. A **467**, 864 (2001).
[10] J.B. Kortright, D.D. Awschalom, J. Stöhr, S.D. Bader, Y.U. Idzerda, S.S.P. Parkin, I.K. Schuller, and H.C. Siegmann, J. Magn. Magn. Mater. **207**, 7 (1999).
[11] D. Weller, *The Physics of Ultrahigh Density Magnetic Recording* (Springer, Berlin, 2001).
[12] J. Stöhr, H.A. Padmore, S. Anders, T. Stammler, and M.R. Scheinfein, Surf. Rev. Lett. **5**, 1297 (1998).
[13] J. Stöhr, Y. Wu, B.D. Hermsmeier, M.G. Samant, G.R. Harp, S. Koranda, D. Dunham, and B.P. Tonner, Science **259**, 658 (1993).
[14] J. Stöhr, J. Magn. Magn. Mater. **200**, 470 (1999).
[15] C.T. Chen, Y.U. Idzerda, H.J. Lin, N.V. Smith, G. Meigs, E. Chaban, G.H. Ho, E. Pellegrin, and F. Sette, Phys. Rev. Lett. **75**, 152 (1995).
[16] H. Mertins, F. Schäfers, X. LeCann, A. Gaupp, and W. Gudat, Phys. Rev. B **61**, R874 (2000).
[17] H.C. Mertins, F. Schäfers, and A. Gaupp, Europhys. Lett. **55**, 125 (2001).
[18] H.A. Dürr, E. Dudzik, S.S. Dhesi, J.B. Goedkoop, G.v. Laan, M. Belakhovsky, C. Mocuta, A. Marty, and Y. Samson, Science **284**, 2166 (1999).
[19] A. Rahmim, S. Tixier, T. Tiedie, S. Eisebitt, M. Lörgen, R. Scherer, W. Eberhardt, J. Lüning, and A. Scholl, Phys. Rev. B **65**, 235421 (2002).
[20] K. Chesnel, M. Belakhovsky, F. Livet, S.P. Collins, G. van der Laan, S.S. Dhesi, J.P. Attane, and A. Marty, Phys. Rev. B **66**, 172404 (2002).
[21] K. Chesnel, M. Belakhovsky, S. Landis, B. Rodmacq, J.C. Toussaint, S.P. Collins, G. van der Laan, E. Dudzik, and S.S. Dhesi, Phys. Rev. B **66**, 024435 (2002).
[22] M.S. Pierce, R.G. Moore, L.B. Sorensen, S.D. Kevan, O. Hellwig, E.E. Fullerton, and J.B. Kortright, Phys. Rev. Lett. **90**, 175502 (2003).
[23] B. Hu, P. Geissbuhler, L.B. Sorensen, S.D. Kevan, J.B. Kortright,

and E.E. Fullerton, Synchrotron Radiat. News **14**, 11 (2001).
[24] J.P. Hannon, G.T. Trammell, M. Blume, and D. Gibbs, Phys. Rev. Lett. **61**, 1245 (1988).
[25] S.W. Lovesey and S. Collins, *X-Ray Scattering and Absorption by Magnetic Materials* (Oxford University Press Inc., New York, 1996).
[26] J.B. Kortright, S.K. Kim, G.P. Denbeaux, G. Zeltzer, K. Takano, and E.E. Fullerton, Phys. Rev. B **64**, 092401 (2001).
[27] *Laser Speckle and Related Phenomena*, edited by J.W. Goodman (Springer, New York, 1984), 2nd ed.
[28] D. Abernathy, G. Grübel, S. Brauer, I. McNulty, G.A. Stephenson, S.G.J. Mochrie, A.R. Sandy, N. Mulders, and M. Sutton, J. Synchrotron Radiat. **5**, 37 (1998).
[29] J. Miao, T. Ishikawa, E.H. Anderson, and K.O. Hodgson, Phys. Rev. B **67**, 174104 (2003).
[30] R. Pecora, *Dynamic Light Scattering: Applications of Photon Correlation Spectroscopy* (Plenum, New York, 1985).
[31] W. de Jeu, B. Osttrovskii, and A. Shalaginov (unpublished).
[32] A.C. Price, L.B. Sorensen, S.D. Kevan, J. Toner, A. Poniewierski, and R. Holyst, Phys. Rev. Lett. **82**, 755 (1999).
[33] C. Gutt, T. Ghaderi, V. Chamard, A. Madsen, T. Seydel, M. Tolan, M. Sprung, G. Grübel, and S. Sinha, Phys. Rev. Lett. **91**, 076104 (2003).
[34] G. Denbeaux, P. Fischer, G. Kusinski, M. Le Gros, A. Pearson, and D. Attwood, IEEE Trans. Magn. **37**, 2764 (2001).
[35] The sample was designed and prepared by O.H. and E.E.F.
[36] The image was recorded by G.D. with the XM-1 x-ray microscope on beam line 6.1.2 at the Advanced Light Source in Berkeley. For an overview on magnetic imaging with this instrument see Ref. 34.
[37] The pinhole was fabricated by C.T.R.